Current Science
CS 4 (4), 603– 614 (2024)
Received 15 May 2024 | **Revised** 26 June 2024 | **Accepted** 25 July 2024 | **Online Available** 18 August 2024
https://doi.org/10.52845/CS/2024-4-4-3

Current Science

Current Science

OPEN ACCESS

ISSN (O) 2795-8639

ORIGINAL ARTICLE

Motion Artifact Correction in Fnirs Signals Based on Spline Interpolation and Locally Weighted Regression

Shuqi Fang[1], Zhiming Xing[2], Boyi Cao[1], Jun Wang[3], Xiumin Gao[1], Xiangmei Dong[1*]

[1]School of Optical-Electrical and Computer Engineering, University of Shanghai Science and Technology, Shanghai 200093, China

[2]School of Information Science and Engineering, Linyi University, Shandong 276000, China

[3]Shanghai Yangpu Mental Health Center, Shanghai 200433, China

Corresponding Author: Xiangmei Dong

Abstract:
Functional near-infrared brain imaging (fNIRS) is a novel, noninvasive technique for brain function testing. The relative motion between the light source detector and the scalp is the main source of motion artifacts, including spike artifacts, slow drift and baseline mutation, which can seriously affect the signal quality. In order to remove the effects of motion artifacts, this paper proposes a hybrid "Spline-Loess (SPLS)" correction algorithm, which effectively removes all types of artifacts in time series signals. First, the baseline drift and spike artifacts present in the signal are identified by the moving standard deviation (MSD) detection method. The drifting signal is then corrected by fitting through cubic spline interpolation, and finally the spikes are removed by smoothing the artifact signal region using a locally weighted regression algorithm. In this paper, an adaptive algorithm is designed for the selection of the parameters of the weighting function in the original local weighted regression: the bandwidth parameter *h* of the weighting function will be determined by the standard deviation of all the signals in the segment to be smoothed. Different types of artifacts are added to the resting-state signal, and then the "SPLS" algorithm is used to correct the signal, and the Pearson's coefficient (R), the absolute mean-square error (RMSE), and the peak error (E_p) are used to compare with the existing seven correction methods. After the experiment, it is found that the two indexes R=0.824 and RMSE=1.78 of the corrected signal using the "SPLS" algorithm, which achieve the best filtering effect compared with other methods.

Keywords: Functional near-infrared spectroscopy (fNIRS); motion artifacts; artifact correction; locally weighted regression; spline interpolation

Introduction

Over the last two decades, functional near-infrared spectroscopic brain imaging (fNIRS) has increasingly gained public attention as a noninvasive and portable neuroimaging technique [1]. It uses near-infrared light to penetrate the scalp to monitor functional brain activity by measuring changes in blood oxygen levels in brain tissue. Compared to electroencephalography (EEG) and magnetic resonance imaging (fMRI), it has higher spatial resolution with lower cost and is less sensitive to artifacts [2-4]. It uses near-infrared light of two different wavelengths (735mm and 850mm used in this paper), emitted from a light source immediately above the scalp, and converts it using a modified version of Beer-Lambert's law to changes in the concentration of oxygenated hemoglobin (HbO) and deoxyhemoglobin (HbR) concentration changes [5-6]. Concentration changes

are reflected as changes in neuronal activation in the superficial cortical layers to monitor hemodynamic changes associated with neural activity in the brain [7-9].

Avoiding random movement of the light source is the most direct way to ensure measurement accuracy. However, motion artifacts can be caused by external factors during the process, such as head bobbing, body shaking, etc. This can lead to sudden changes in the amplitude of the received signal, which can result in different types of artifacts. Spike artifacts are usually large changes in amplitude over a short period of time and quickly return to the original amplitude and can be considered as impulse type signals. Generally speaking, the amplitude of spike artifacts can be up to two orders of magnitude larger than the normal signal, and these artifacts can be corrected by smoothing filtering. Baseline drift is similar to a step signal, and this type of artifact can be subdivided into two types: abrupt baseline change and slow drift. When this type of artifact occurs, the signal baseline will change from one amplitude to another and will not return to its original amplitude [10-12]. These artifact signals have become one of the important factors affecting image quality and visualization results. Therefore, how to accurately remove motion artifacts is a challenging topic nowadays.

In the initial stage of research, the general choice is to discard the abnormal signal channels, but this is not desirable in the case of a small number of experiments [6]. To solve this problem, researchers have gradually proposed numerous artifact removal techniques and methods, including hardware-based processing methods, image processing algorithms, and so on. They can be categorized into methods based on the temporal characteristics of the signal, methods based on the spatial characteristics of the signal, and the removal of motion artifacts from external signals using adaptive filters [13-14]. However, each of these algorithms has its own scope of application and limitations.

The wavelet method involves wavelet transforming the original signal to obtain the wavelet coefficients, removing motion artifacts by removing the corresponding wavelet coefficients, and wavelet inversion to reconstruct the entire signal sequence [15]. It is effective in eliminating spiky artifacts, but also exacerbates baseline artifacts [16-17]. Principal component analysis (PCA), which can be used to extract the main feature components of a signal, corrects the signal by removing the first n components from the signal. However, principal component analysis methods applied to whole-segment measurement signals tend to poorly separate brain signals from motion artifacts and also tend to overcorrect the signal [18-19]. Target Principal Component Analysis (tPCA), an algorithm developed to avoid PCA overcorrection, but relies on the detection of artifacts and requires the user to set many parameters [20]. Correlation-based signaling improvement (CBSI) has the strong assumption that HbO and HbR generated in the brain are always negatively correlated, an assumption that does not hold in many cases [11]. Spline interpolation is a local fitting technique. It approximates the unknown values between data points by fitting the signal with polynomials, and is able to correct baseline drift artifacts well. However, the method relies on the accurate detection of artifactual movie segments and is ineffective for spike-type artifacts [21-22].

Local weighted regression (Loess), a nonparametric regression method, assigns different weights to the data points near each prediction point, thus making the fitted signal more closely match the actual data, which achieves a smooth filtering of the signal and removes high-frequency motion artifacts. However, since each point needs to be involved in the regression, it is computationally intensive and relatively ineffective in removing baseline drift [23]. The core of the algorithm is the computation of the weight function, which assigns a different weight to each point [24-25]. Therefore, for the selection of the parameters in the weight function, it will greatly affect the effectiveness of the filtering.

After analyzing the characteristics of many previous filtering techniques, an ideal motion artifact removal technique needs to be able to process both spike artifacts and baseline drift artifacts, so as to ensure that the corrected signals can adequately respond to the hemodynamic response of the subject's neural activity. Based on this goal, this paper proposes the “SPLS algorithm”, under the premise that the spline interpolation method effectively removes baseline drift, the smoothing effect is also optimized by

adaptively selecting the parameters of the weighting function in the local weighted regression algorithm.

1. SPLS Motion Artifact Removal Algorithm

The main purpose of the SPLS algorithm is to effectively remove motion artifact signals such as baseline drift and spikes from the signal, while restoring the true hemodynamic response of the human body. The correction of motion artifacts can be divided into three major steps: identification, correction, and reconstruction.

The algorithm identifies the baseline drift in the whole time series signal using percentiles after first calculating the moving standard deviation of the signal. For the baseline drift portion, it is corrected by fitting a cubic spline interpolation function, which is subtracted from the original signal. Subsequently, the signal segments are smoothed using locally weighted regression, which adaptively determines the optimal bandwidth parameter *h* of the weighting function through the characteristics of the signal region, improving the overall effect of smoothing.

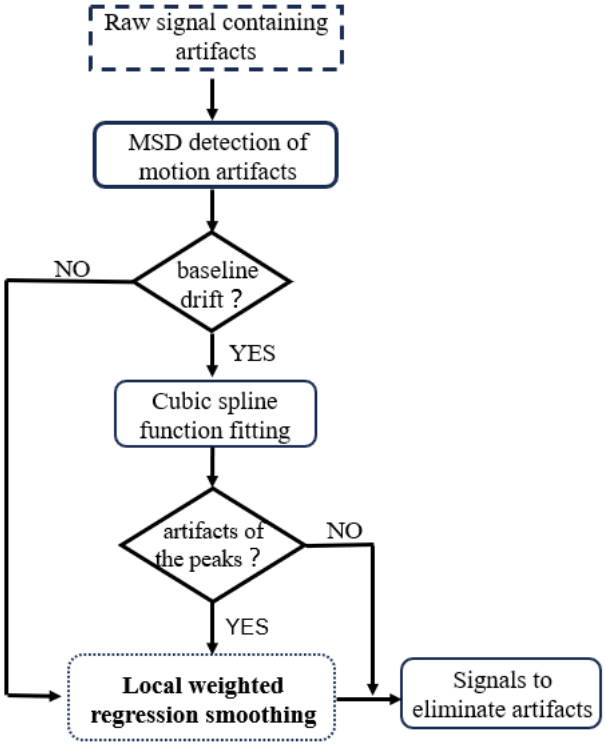

Figure 1. A schematic depiction of SPLS algorithm's processing stream.

1.1 MSD Detection Algorithm

The moving standard deviation is first utilized to detect the presence of motion artifact signals in the entire time series. It is a statistical measure of the degree of variability in the data and is commonly used for smoothing time series data as well as volatility analysis, which can help identify trends and unusual fluctuations in the data. The formula for the two-sided moving standard deviation is as follows:

$$s(t)=\frac{1}{2k+1}\left[\sum_{j=-k}^{k}x^2(t+j)-\frac{1}{2k+1}\left(\sum_{j=-k}^{k}x(t+j)\right)^2\right]^{\frac{1}{2}} \quad (1)$$

Where *W* is the sliding window size, *W=2k+1*. *t=k+1, k+2, …, N-K*, where *N* is the length of the time series, *j=3FS*, *FS* is the sampling rate.

In this detection method, the threshold of MSD is a key parameter that needs to be set, which will directly affect the recognition effect of artifacts. After calculating the moving standard deviation of the signal, the corresponding threshold needs to be set to mark the part where the artifacts appear. This part utilizes the percentile method to select the appropriate threshold value. Percentile is a method in statistics. It is defined as ranking a set of data from smallest to largest and calculating the corresponding cumulative percentile; the value of the data corresponding to a particular percentile is called the percentile. This can be expressed as a

set of observations arranged in numerical order, for example, the value at position *p%* is called the *p* percentile.

Different percentiles can be obtained for different identification thresholds *T*. The artifact signal segments identified by the threshold *T* are compared with known artifact segments, and the percentile corresponding to the smallest error is taken as the best value. The expression of this error calculation method is shown in the following equation.

$$Error = \frac{\left|L_{indentified} - L_{sample}\right|}{L_{sample}} \times 100\% \qquad (2)$$

where $L_{indentified}$ is the length of the signal segment recognized by the threshold *T*. L_{sample} is the length of the known artifact segment. According to the experimental results of Zhou et al. when the percentile of *T* is 95, the recognition effect of motion artifacts can reach the best [4]. Therefore, in this paper, P_{95} will be taken for recognition, and the expression for threshold selection is as follows:

$$T = \sqrt{P_{95} \times MSD_{average}} \qquad (3)$$

P is the percentile in the MSD series and $MSD_{average}$ is the mean of the MSD series.

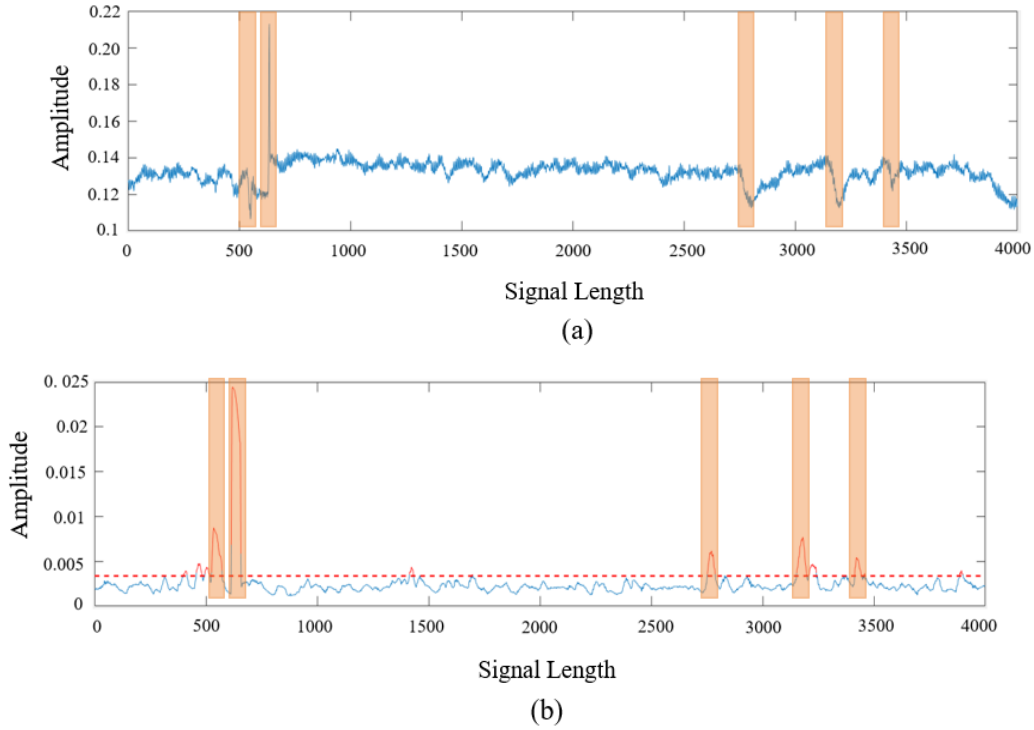

Figure 2. Results for motion artifact recognition. (a) Simulation of randomly generated signal segments containing motion artifacts; (b) Identified motion artifacts using the 95th percentile obtained with a threshold of 0.003

1.2 Spline Interpolation

The baseline drift in the signal is first removed using cubic spline interpolation. The algorithm is mainly divided into the following steps:

(i) Identify the baseline drift in the signal and determine the start and end points of each drift. With the hybrid detection algorithm described above, the baseline drift and spike artifacts in the signal have been identified.

(ii) For the detected motion artifact sequence, the cubic spline interpolation function is applied. A cubic polynomial is fitted in each interval, boundary conditions are set to obtain a system of equations, and the coefficients of each subinterval are derived. Finally, given the interpolation points, the coefficients are used to find the corresponding function values.

(iii) The sequence of signals in the presence of baseline drift is subtracted from the triple spline interpolation fit to obtain a new segment of filtered signal.

1.3 Locally weighted regression algorithm

For the spiky artifacts detected by the above proposed method, we use local weighted regression (Loess) to remove them. The algorithm is a point-by-point weighted regression smoothing algorithm, for each corresponding signal value of the original data, a number of neighboring known signal values can be used, and it is necessary to obtain the weight matrix corresponding to the *i*th signal value, then the loss function in linear regression becomes [23]:

$$f(\theta)=\sum_{i=1}^{n}\omega_i\left(y_i-x_i{}^T\theta\right)^2 \qquad (4)$$

Eventually it can be inversely solved for θ:

$$\theta=\left(x^T\omega x\theta\right)^{-1}x^T\omega y \qquad (5)$$

Where x_i is the signal point and y_i is the target value to be predicted. So as long as the weights ω of each signal point are known, then the rest is the same as standard linear regression to find the regression coefficient θ. This paper will use the Tricube weight function, which is characterized as decreasing with distance [26]. A quadratic polynomial is then fitted using those data points with weights greater than zero to obtain a local best-fit curve. This function can be expressed as:

$$w=\left(1-\left|\frac{x-x(i)}{h}\right|^3\right)^3 \qquad (6)$$

w denotes the weight function and h is an important parameter in this function that controls the rate at which the weights decrease with distance. This function takes the maximum value of 1 when $x=x_i$ and will treat the weights of the predicted points as 0 when $|x-x_i|>h$. The weighting function reduces the effect of data far from the fitted point, thus making the fitting more focused on localized data. In the process of filtering using this algorithm, since the bandwidth h of the weighting function needs to be set manually by human beings, a constant value will not be able to deal with time series signals with different trends most efficiently. Therefore, an adaptive method for selecting the bandwidth parameter *h* is proposed in this paper:

In the signal interval to be smoothed, the standard deviation of all signal values in the interval is calculated, and the calculated value is used as the parameter h in the above equation.

This local bandwidth *h* will be used to determine a key parameter in the local regression that affects the degree of smoothing at each point. An important characteristic of this optimization method is its ability to adapt to the local density of the data points, which makes it possible to automatically select smaller bandwidths in regions of smaller data volatility; and larger bandwidths in regions of larger data volatility, thus achieving effective noise suppression while maintaining the original characteristics of the signal.

1.4 Evaluation methods and indicators

In order to be able to more intuitively see the correction effect of each filtering algorithm, the signals with motion artifacts will be processed by using the SPLS algorithm, spline interpolation, wavelet filtering, SG filtering, TDDR, spline - wavelet, and spline -SG, which are a total of seven correction methods proposed in this paper, respectively. Finally, the processed signal is quantitatively compared with the original resting state reference signal. The following three metrics were used for comparison: 1. Root Mean Square Error (RMSE); 2. Pearson's coefficient (R); 3. Peak Error (E_p)

$$RMSE=\sqrt{\frac{1}{N}\sum_{i=1}^{n}\left(y_i-x_i\right)} \qquad (7)$$

$$r=\frac{\sum_{i=1}^{n}(x_i-\bar{x})(y_i-\bar{y})}{(n-1)s_xs_y} \qquad (8)$$

$$MAX\left(\left|x(t_i)-y(t_i)\right|\right) \qquad (9)$$

Where $x(t_i)$ is the signal corrected for artifacts, $y(t_i)$ is the original signal after acquisition, and s_x and s_y are the standard deviations of the two signals. These three indexes are mainly a measure of the difference between the original signal and the corrected signal.

1.5 Construction of resting-state fNIRS data with artifact signals

A total of 22 subjects were called to participate in our experiment (12 subjects were male and 10 were female. The average age was 25 years). All subjects were healthy students with no previous

history of neurological or psychiatric illnesses. All participants signed an informed letter and the protocol was approved by the Ethics Committee of University of Shanghai Science and Technology.

The experimental environment was chosen to be in a room with low light and good soundproofing to minimize the disturbance of the external environment to the test subjects. Subjects were asked to remain calm and relaxed in a supine position for 5 minutes to eliminate as much as possible the effects of the active behavior prior to the experiment. Such a set of experiments lasted 16 minutes, during which the subjects were asked to remain calm and not to move their heads significantly. We repeat 3 sets of a complete experiment for a total of 48 minutes, and finally obtain a resting-state brain signal dataset. The experiments were performed using a near-infrared brain imaging system developed by the group, which contains two dual-wavelength light sources (light source wavelengths of 735 nm and 850 nm), and eight long-distance detection channels (light source and detector 3 cm apart, single-detector measurement mode). The hardware system includes a cerebral blood oxygen acquisition circuit, a light source-detector module and a data acquisition module. Two wavelengths of near-infrared light were flashed alternately to collect signals, and the sampling rate was set to 10HZ to measure the concentration changes of oxygenated hemoglobin (HbO) and deoxyhemoglobin (HbR) in the prefrontal cortex. In this experiment, the positioning of the light source to the detectors was based on the position of Fp2 in the EEG 10-20 system [27-28], with a distance of 3 cm from the surrounding detectors.

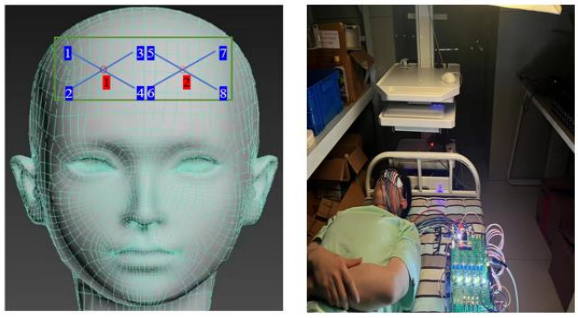

Figure 3. Photographs of the light source and detector array locations and signal acquisition. The left figure shows the distribution position of the 2 light sources with 8 detectors in the prefrontal lobe; the right figure shows the resting state signal acquisition by the author

In this paper, among a large number of data signals collected, 20 groups of smooth resting-state signal data are selected as reference signals for algorithm comparison. According to the artifact characteristics, several data sets containing different types of motion artifacts are simulated and generated. Moreover, the simulated spike-type artifacts and baseline drift artifacts are added in the selected resting-state data sets ranging from 1 to 5 groups respectively in order to make the algorithm comparison results more general.

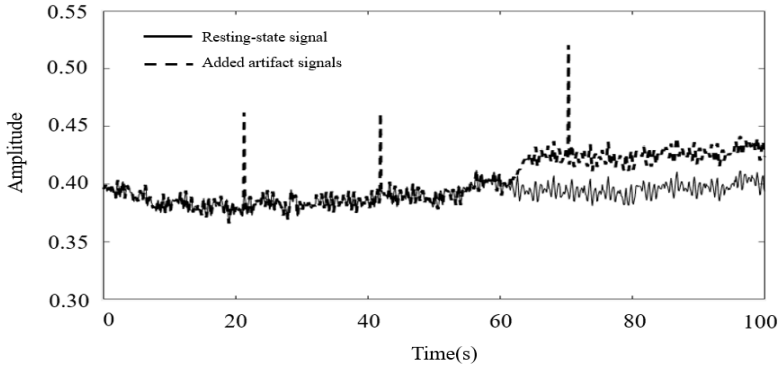

Figure 4. Raw resting-state data and signal after adding motion artifacts

2. Experimental results and analysis

In the previous section, a complete set of SPLS algorithms is proposed, from the process of recognizing motion artifacts to the removal of baseline drift and spike artifacts. This section is divided into two parts: firstly, for the recognized spike artifacts, different smoothing intervals are taken for testing, and the effect of different interval lengths on the smoothing effect is verified. Then the filtering effect of the SPLS algorithm is quantitatively compared with seven other filtering algorithms, which enables a more objective evaluation of the performance of the proposed algorithm.

2.1 Selection of smoothing range for locally weighted regression

In this study, the effect of different choices of smoothing ranges on the treatment of spike artifacts in the locally weighted regression model is experimentally verified. After the spike artifact is identified by the above method, a smaller signal fragment is then extended to the left and right ends of the spike point, and the extended artifact interval is locally weighted smoothed. The sampling rate of the signal is 10HZ, and the duration of the test extension is 1~4s.

Table 1. Extended different signal lengths to test the smoothing effect of the SPLS algorithm. Each extended length of time was processed with 10 different sets of spiked signal segments and the average results of the final metrics are shown in the table below.

Extended duration	R	RMSE ($\times 10^3$)
1s	0.863(0.858~0.892)	2.72(1.97~3.30)
2s	0.870(0.852~0.898)	**2.61(1.77~2.96)**
3s	**0.873(0.856~0.897)**	2.67(1.87~3.01)
4s	0.868(0.850~0.890)	2.63(1.73~2.90)

By processing multiple sets of data, as shown in the experimental results in Table 1 above, the different length segments do have some effect on the locally weighted regression smoothing, but the overall smoothing effects are all relatively close to each other. The RMSE showed the best results in the length of the signal with 2s taken at each end of the smoothing, while R reached the best in the signal with 3s taken at each of the two segments. Therefore, on the premise that there is no large difference in interval selection, the time series signals with 2s taken at each end of the identified spike artifacts will be processed in the subsequent processing of the spike artifact signals.

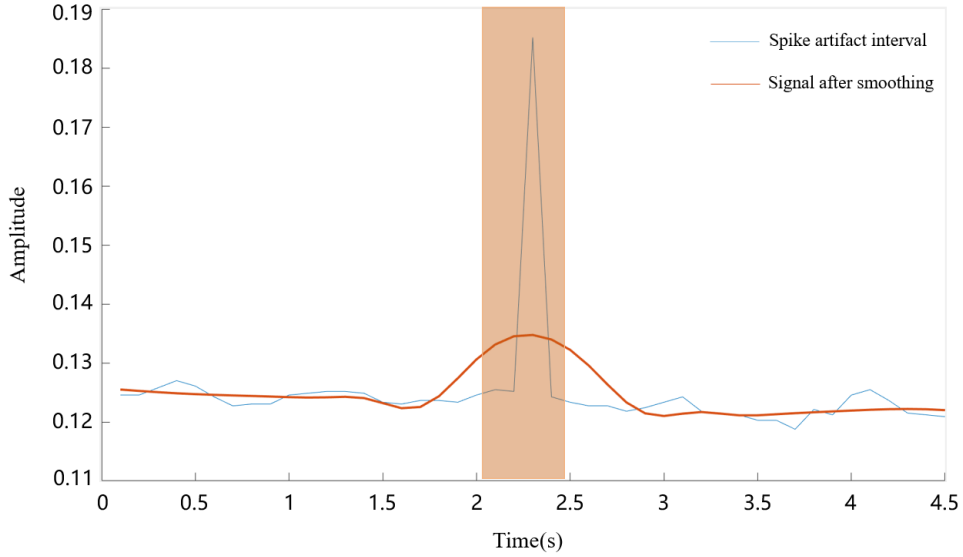

Figure 5. The orange box shows the MSD detected spike signal, where a 2s signal sequence was extended in each of the two segments of the region and the artifact segment was smoothed.

2.2 Comparison of SPLS algorithm with other filtering algorithms

Figure6 demonstrates the entire filtering process of the SPLS algorithm. Figure (a) shows the acquired resting-state signal, of which 300s of data was selected. To the above signal, 4 spike artifacts, 2 segments of baseline mutation with 2 segments of slow drift consisting of artifact-containing signal segments are added as shown in (b). Then the drift segments were removed using cubic spline interpolation fitting; the local weighted regression algorithm smoothed the selected signal regions, and the final results are shown in Figure (d).

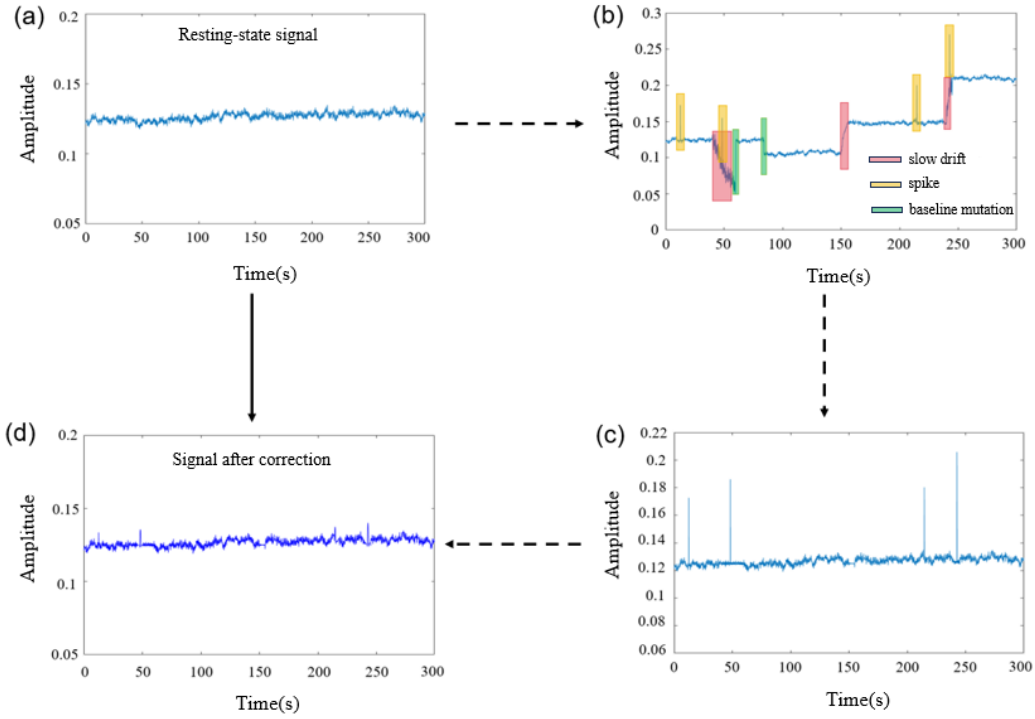

Figure 6. Processing diagram of the SPLS algorithm. (a) Acquired resting-state signals; (b) manually added various types of motion artifact clips and detected artifact signals by MSD, using the 95th percentile selection threshold; (c) results of spline interpolation to correct baseline drift; (d) results after local weighted regression smoothing

In order to visualize the effect of different correction methods in removing motion artifacts, this paper compares seven correction methods by the SPLS method with Spline, SG, Wavelet, Loess, TDDR, Spline-SG, and Spline-Wavelet as shown in Figure 7.The Spline method is effective in correcting offset-type artifacts but is not effective for the Spline is effective in correcting offset artifacts, but is ineffective for high-frequency spike artifacts, and Spline leaves residuals at the beginning and the end of the artifact segment. TDDR is an effective correction for baseline drift and does not introduce residuals, but it is ineffective for spike-type artifacts. Wavelet effectively removes spikes in the signal, but this removes spikes and leads to baseline drift of the signal at the same time. The S-G and Loess methods eliminate residual spikes, but have no effect on baseline drift in the signal. In contrast, the Loess method is better than SG and Wavelet in tracking the original signal trend during the time period when there is a baseline shift. SPLS, Spline-SG, and Spline-wavelet are good combinations of methods that can eliminate the baseline drift and high-frequency spikes in the measurement results. The "SPLS" method mentioned in this section is significantly better than the comparison method in removing the high-frequency spike artifacts.

In Table 2 below, the correlation coefficients with the resting-state signals after removing the artifacts using different correction methods are shown (the bolded part indicates the best value of the coefficients). After filtering 20 simulated artifact signals with different methods, the average values of Pearson's correlation coefficient and root-mean-square error of the proposed SPLS algorithm are 0.824 and 0.00178, respectively, and the corrected signals have the best linear correlation with the original resting-state signals.

In the peak error, the maximum peak error of the corrected signal with the "Spline-wave" method is best controlled with the resting state signal. The SPLS method shows the best results in removing different motion artifacts from the signal by adding different amounts of artifacts.

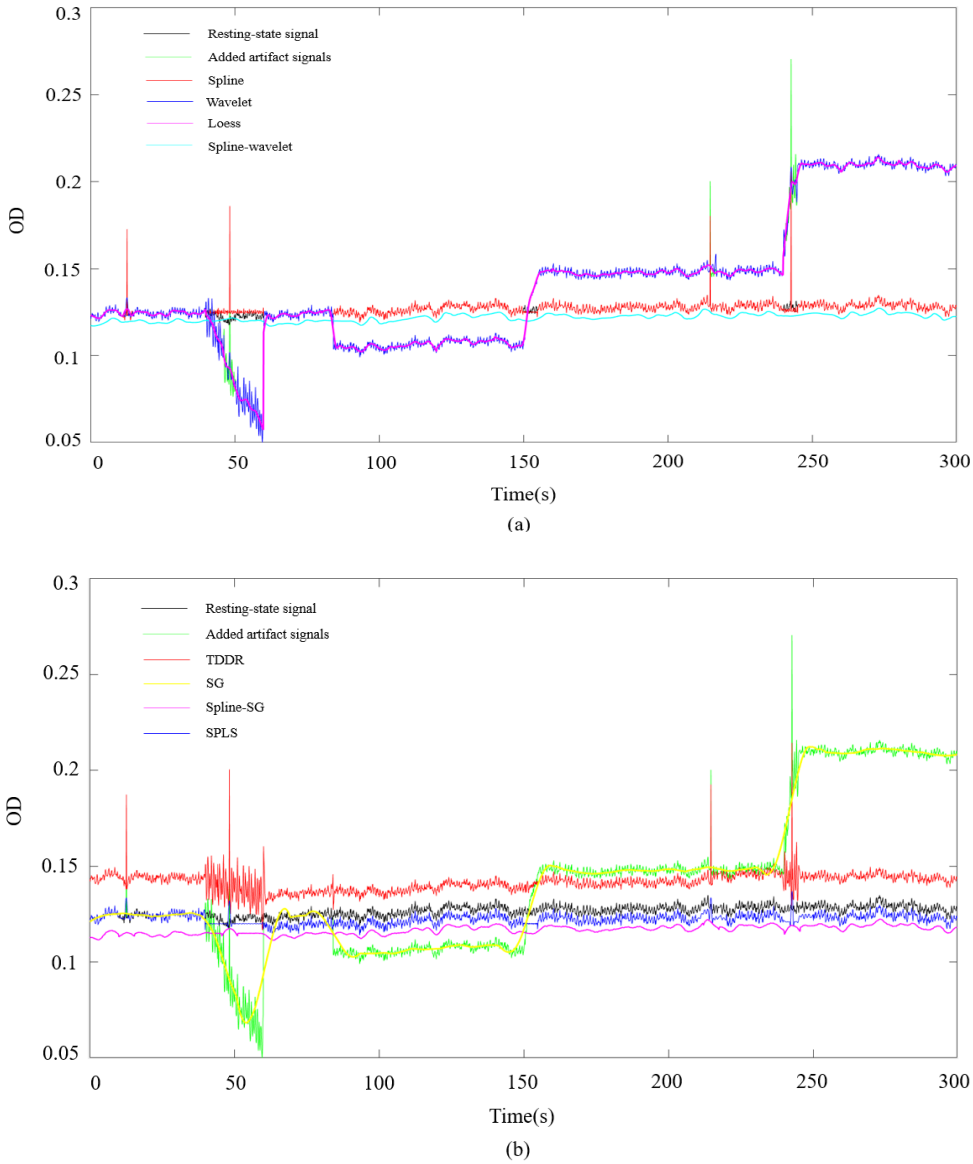

Figure 7. Effect of different correction methods on motion artifact removal, where black is the acquired resting-state signal and green is the signal after adding different types of motion artifacts manually

Table 2. Results of metric comparison of 20 groups of simulated artifact signals with resting-state signals using three metrics, R, RMSE, and E_p

Methods	R	RMSE ($\times 10^3$)	E_P
No correction	0.638(0.545~0.675)	3.29(1.61~5.09)	0.067(0.05~0.1)
Spline	0.710(0.652~0.796)	2.72(1.29~4.61)	0.07(0.05~0.1)
SG	0.728(0.661~0.772)	2.74(0.741~3.95)	0.03(0.0039~0.0655)
Wavelet	0.703(0.634~0.763)	2.88(0.783~4.40)	0.03(0.0048~0.0864)
Loess	0.734(0.701~0.792)	2.56(0.712~3.2)	0.025(0.0033~0.052)
TDDR	0.745(0.727~0.767)	2.35(0.864~3.82)	0.04(0.012~0.073)
Spline-SG	0.804(0.753~0.836)	1.95(0.629~3.93)	0.0074(0.0018~0.013)
Spline-wave	0.798(0.763~0.822)	1.92(0.614~3.687)	**0.0071(0.002~0.014)**

SPLS	**0.824(0.791~0.856)**	**1.78(0.5595~3.367)**	0.0080(0.003~0.010)

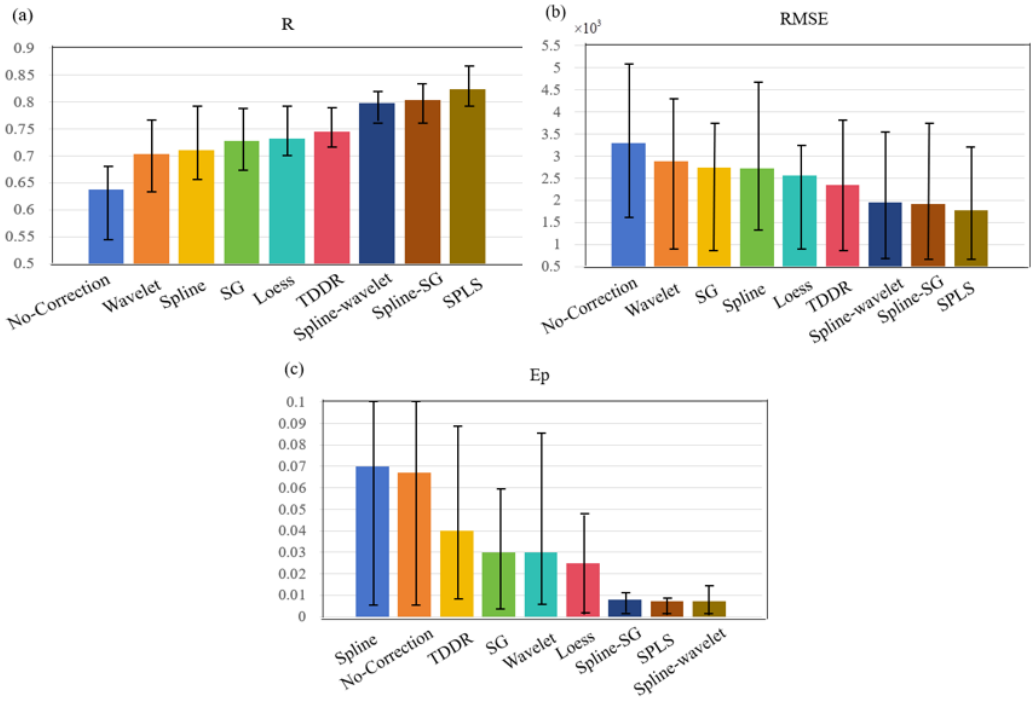

Figure 8. Compares the performance of seven different correction methods for removing motion artifacts. (a) R, (b) RMSE, (c) E_p, where the bars indicate the mean values and the error lines indicate the standard errors

3. Discussion

In previous studies, locally weighted regression was mainly used for smoothing and trend modeling in statistical and data analysis. This method was utilized in the removal of motion artifacts, with the earliest application being in medical imaging, specifically magnetic resonance imaging (MRI) [29-31]. Motion artifacts in imaging are caused by patient motion, and the use of locally weighted regression can help to smooth the image and minimize the effects of these artifacts. During the calculation of the weighting function, the value of the bandwidth parameter *h* will directly affect the effectiveness of the smoothing correction of the signal, resulting in differences in the artifact correction effect, and a constant parameter will not be able to most effectively handle time series signals with different trends. In this paper, the smoothing method is applied to deal with motion artifacts in fNIRS signals, and based on this, the "SPLS" hybrid correction method is proposed. The method solves the problem of setting parameters manually, and will automatically select the parameters according to the trend characteristics of the local signal to achieve the best correction effect.

In this paper, in order to avoid the chance of removing artifacts due to insufficient data, brain signals from a total of 22 subjects were tested for 45 minutes per experiment, with a sufficient amount of signal data to be used as a comparative reference signal after artifact correction, in order to compare the correction effects of different methods. Thereafter, different types and amounts of motion artifacts were added to the acquired resting-state data as the signals to be corrected. We compare the proposed algorithm with seven commonly used correction methods in previous studies, and the results show that the SPLS algorithm outperforms these commonly used methods by significantly improving the Pearson's coefficient between the resting-state signals and the reference signals, and decreasing RMSE between them.

The results of testing the different correction methods (Figure 7) show that Spline Interpolation-SG, Spline Interpolation-Wavelet, and SPLS are significantly better than the other methods, with SPLS being the most effective.

Combined filtering methods can smooth out the spikes in the signal while treating the baseline drift, and have become the main artifact correction method used by researchers today[31]. Spline interpolation has an outstanding ability to suppress the baseline drift, but there are significant residuals when the signal is reorganized. Methods such as SG and wavelet can remove spikes but have no direct effect in terms of baseline mutation.

In applying the SPLS algorithm, the most important limitation of the smoothing process is that it is very costly in terms of computational time and sensitive to outliers, due to the choice of a local weighting method. Each point requires the calculation of its corresponding weight value, thus also greatly increasing the computational effort.

4. Conclusion

In this paper, a hybrid "SPLS" correction method is proposed to remove motion artifacts from fNIRS signals. Spline interpolation is used to correct for baseline drift, and locally weighted regression is used to smooth out spikes. On this basis, in this paper, an adaptive selection algorithm of parameters is designed in the local weighted regression, and the parameter *h* of the weight function will be determined according to the degree of fluctuation of the local signal. Finally, three common metrics (R, RMSE, E_p) for motion artifact correction are verified, and the results show that the "SPLS" method proposed in this paper has the best effect in correcting motion artifacts in fNIRS signals.

Data Availability Statement: Data Availability Statement: The data behind the results of this paper has been deposited in a laboratory database and is available to a wide range of researchers.

Informed Consent Statement: Informed consent was obtained from all participants in the study. Participants' personal data are protected by the "Non-Profit Ordinance"

Conflicts of Interest: The authors declare no conflicts of interest.

References

1. Jobsis F F N. Infrared Monitoring of Cerebral and Myocardial Oxygen Sufficiency and Circulatory Parameters[J]. Science, 1977,198: 1264.
2. Fishburn F A, Ludlum R S, Vaidya C J, et al. Temporal derivative distribution repair (TDDR): a motion correction method for fNIRS[J]. Neuroimage, 2019, 184: 171-179.
3. Hiroyasu T, Nakamura Y, Yokouchi H. Method for removing motion artifacts from fNIRS data using ICA and an acceleration sensor[C]//2013 35th Annual International Conference of the IEEE Engineering in Medicine and Biology Society (EMBC). IEEE, 2013: 6800-6803.
4. Farago E, Chan A D C. Motion artifact synthesis for research in biomedical signal quality analysis[J]. Biomedical Signal Processing and Control, 2021, 68: 102611.
5. Kocsis L, Herman P, Eke A. The modified Beer–Lambert law revisited[J]. Physics in Medicine & Biology, 2006, 51(5): N91.
6. Baker W B, Parthasarathy A B, Busch D R, et al. Modified Beer-Lambert law for blood flow[J]. Biomedical optics express, 2014, 5(11): 4053-4075.
7. Pinti P, Tachtsidis I, Hamilton A, et al. The present and future use of functional near-infrared spectroscopy (fNIRS) for cognitive neuroscience[J]. Annals of the New York Academy of Sciences, 2020, 1464(1): 5-29.
8. Lloyd-Fox S, Blasi A, Elwell C E. Illuminating the developing brain: the past, present and future of functional near infrared spectroscopy [J]. Neuroscience & Biobehavioral Reviews, 2010, 34(3): 269-284.
9. Yang M, Xia M, Zhang S, et al. Motion artifact correction for resting-state neonatal functional near-infrared spectroscopy through adaptive estimation of physiological oscillation denoising[J]. Neurophotonics, 20 22, 9(4): 045002.
10. Gao L, Wei Y, Wang Y, et al. Hybrid motion artifact detection and correction approach for functional near-infrared spectroscopy measurements[J]. Journal of Biomedical Optics, 2022, 27(2): 025003-025003.
11. Novi S L, Roberts E, Spagnuolo D, et al. Functional near-infrared spectroscopy for speech protocols: characterization of motion artifacts and guidelines for improving data analysis[J]. Neurophotonics, 2020,7(1):01500 1.
12. Barker J W, Rosso A L, Sparto P J, et al. Correction of motion artifacts and serial

correlations for real-time functional near-infrared spectroscopy[J]. Neurophotonics, 20 16, 3(3): 031410-031410.
13. Cui X, Bray S, Reiss A L. Functional near infrared spectroscopy (NIRS) signal improvement based on negative correlation between oxygenated and deoxygenated hemoglobin dynamics[J]. Neuroimage, 2010, 49(4): 3039-3046.
14. Cooper R J, Selb J, Gagnon L, et al. A systematic comparison of motion artifact correction techniques for functional near-infrared spectroscopy[J]. Frontiers in neuroscience, 2012, 6: 147.
15. Singh B N, Tiwari A K. Optimal selection of wavelet basis function applied to ECG signal denoising[J]. Digital signal processing, 2006, 16(3): 275-287.
16. Huang R, Hong K S, Yang D, et al. Motion artifacts removal and evaluation techniques for functional near-infrared spectroscopy signals: a review[J]. Frontiers in Neuroscience , 2022, 16: 878750.
17. Molavi B, Dumont G A. Wavelet-based motion artifact removal for functional near-infrared spectroscopy[J]. Physiological measurement, 2012, 33(2): 259.
18. Zhang Y, Brooks D H, Franceschini M A, et al. Eigenvector-based spatial filtering for reduction of physiological interference in diffuse optical imaging[J]. Journal of biomedical optics, 2005, 10(1): 011014-0110 14-11.
19. Maćkiewicz A, Ratajczak W. Principal components analysis (PCA)[J]. Computers & Geosciences, 1993, 19(3): 303-342.
20. Yücel M A, Selb J, Cooper R J, et al. Targeted principle component analysis: a new motion artifact correction approach for near-infrared spectroscopy[J]. Journal of innovative optical health sciences, 2014, 7(02): 1350066.
21. Brigadoi S, Ceccherini L, Cutini S, et al. Motion artifacts in functional near-infrared spectroscopy: a comparison of motion correction techniques applied to real cognitive data[J]. Neuroimage, 2014, 85: 181-191.
22. Scholkmann F, Spichtig S, Muehlemann T, et al. How to detect and reduce movement artifacts in near-infrared imaging using moving standard deviation and spline interpolation[J]. Physiological measurement, 2010, 31(5): 649.
23. Cleveland W S. Robust locally weighted regression and smoothing scatterplots[J]. Journal of the American statistical association, 1979, 74(368): 829-836.
24. Jahani S, Setarehdan S K, Boas D A, et al. Motion artifact detection and correction in functional near-infrared spectroscopy: a new hybrid method based on spline interpolation method and Savitzky–Golay filtering[J]. Neurophotonics, 2018, 5(1): 015003-015003.
25. Morell O, Otto D, Fried R. On robust cross-validation for nonparametric smoothing[J]. Computational Statistics, 2013, 28(4): 1617-1637.
26. Moreno Á, García-Haro F J, Martínez B, et al. Noise reduction and gap filling of fAPAR time series using an adapted local regression filter[J]. Remote Sensing, 2014, 6(9): 8238-8260.
27. Kim Y W, Kang H B. Eye Movement-based Visual Discomfort Analysis from Watching Stereoscopic 3D Contents Regarding Brightness and Viewing Distance[J]. Journal of Korea Multimedia Society, 2016, 19(9): 17 23-1737.
28. Wang X, Yao L, Zhao Y, et al. Effects of disparity on visual discomfort caused by short-term stereoscopic viewing based on electroencephalograph analysis [J]. Bio Medical Engineering OnLine, 2018, 17: 1-17.
29. Atkinson D, Hill D L G. Reconstruction after rotational motion[J]. Magnetic Resonance in Medicine: An Official Journal of the International Society for Magnetic Resonance in Medicine, 2003, 49(1): 183-187.
30. Di Lorenzo R, Pirazzoli L, Blasi A, et al. Recommendations for motion correction of infant fNIRS data applicable to multiple data sets and acquisition systems[J]. Neuroimage, 2019, 200: 511-527.
31. Ferrari M, Quaresima V. A brief review on the history of human functional near-infrared spectroscopy (fNIRS) development and fields of application[J]. Neuroimage, 2012, 63(2): 92 1-935.